

Surmounting the sign problem in nonrelativistic calculations: A case study with mass-imbalanced fermions

Lukas Rammelmüller,¹ William J. Porter,² Joaquín E. Drut,² and Jens Braun^{1,3}

¹*Institut für Kernphysik (Theoriezentrum), Technische Universität Darmstadt, D-64289 Darmstadt, Germany*

²*Department of Physics and Astronomy, University of North Carolina, Chapel Hill, NC, 27599, USA*

³*ExtreMe Matter Institute EMMI, GSI, Planckstraße 1, D-64291 Darmstadt, Germany*

The calculation of the ground state and thermodynamics of mass-imbalanced Fermi systems is a challenging many-body problem. Even in one spatial dimension, analytic solutions are limited to special configurations and numerical progress with standard Monte Carlo approaches is hindered by the sign problem. The focus of the present work is on the further development of methods to study imbalanced systems in a fully nonperturbative fashion. We report our calculations of the ground-state energy of mass-imbalanced fermions using two different approaches which are also very popular in the context of the theory of the strong interaction (quantum chromodynamics, QCD): (a) the hybrid Monte Carlo algorithm with imaginary mass imbalance, followed by an analytic continuation to the real axis; and (b) the complex Langevin algorithm. We cover a range of on-site interaction strengths that includes strongly attractive as well as strongly repulsive cases which we verify with nonperturbative renormalization group methods and perturbation theory. Our findings indicate that, for strong repulsive couplings, the energy starts to flatten out, implying interesting consequences for short-range and high-frequency correlation functions. Overall, our results clearly indicate that the Complex Langevin approach is very versatile and works very well for imbalanced Fermi gases with both attractive and repulsive interactions.

I. INTRODUCTION

Ultracold quantum gases have given us the opportunity to directly observe many-body physics at work in an unprecedented way. Over the last few decades, with the advent of laser trapping and cooling techniques, experimentalists have progressively achieved a previously unimagined degree of control for a wide range of atomic systems. As a consequence, the variety of quantities that can be measured with precision has grown dramatically [1]. As is now well known, tuning across magnetic Feshbach resonances allows for the interaction strength to be varied essentially at will. Additionally, the fine tuning of optical trapping potentials has enabled the study of lattice models of direct relevance to condensed matter physics [2], including systems in low dimensions (by highly constrained traps). Similarly, the clever use of the internal nuclear states of alkali and alkali-earth atoms has made it possible to probe systems with multiple internal degrees of freedom, i.e. with $SU(N)$ flavor symmetry [3, 4]. Most relevant for this work, experiments involving atomic mixtures of fermionic (or even fermionic *and* bosonic) species has facilitated access to *mass-imbalanced* situations, a case that is interesting for a variety of reasons but has been studied less than its spin-imbalanced counterpart. Recent experimental setups include fermionic mixtures of ^6Li and ^{40}K [5–7]. Moreover, other systems with mixtures of a variety of suitably chosen different fermion species (such as ^6Li , ^{40}K , ^{161}Dy , ^{163}Dy , and ^{167}Er) appear within reach in the future (see, e.g., Refs. [8–10]).

Given the rapid experimental progress, in particular with respect to spin- and mass-imbalanced quantum gases, this work aims at the further theoretical development of stochastic frameworks required for *ab initio* studies of such systems in any dimension. In other words,

with our developments in the present paper, we particularly aim at aspects which can currently only be accessed in a very limited fashion with conventional Monte Carlo (MC) methods, if at all. To test our developments, we examine the equation of state of mass-imbalanced Fermi mixtures when confined to one-dimensional (1D) situations. Although 1D systems are also experimentally relevant (see, e.g., Ref. [11]), we do not aim at a high-precision calculation of the equation of state with our present study. Our goals are rather of methodological nature. From the latter standpoint, the 1D limit is appealing since the running times of the computations are comparatively short and it is therefore possible to take vastly more data than in higher dimensions. This allows to reduce systematic errors (e.g. by studying large lattice sizes) and focus on the underlying methods. Moreover, as is well known, 1D systems of fermions with contact interaction are typically solvable by the Bethe ansatz technique for arbitrary particle numbers [12]. In some cases the analytic investigations have been complemented by numerical studies (see e.g. [13–16]). However, as soon as the system involves particles of general unequal masses, an analytic solution is currently out of reach. While the two-body problem can of course be solved, the solution of mass-imbalanced few-body systems is restricted to special mass configurations [17, 18], or infinite interaction strength [19], or specific boson-fermion mixtures [20]. In any case, the existence of analytic solutions in some cases and the absence of theoretical results in other cases represents a further motivation for the developments discussed in the present work.

It is worth noting that progress has been made in related cases such as the half-filled asymmetric Hubbard model in 1D [21] as well as 3D [22], which does not feature a sign problem and is directly connected to the Falicov-

Kimball model in the limit of large asymmetry (and is thus of interest to a sector of the condensed-matter community). Cases away from half filling were also studied in Refs. [23, 24]. Furthermore, exact diagonalization studies have addressed harmonically trapped systems of up to 10 particles [25, 26]. While these methods provide results for the few-body regime, it is challenging to extend them beyond low particle numbers or to higher dimensions due to the prohibitive scaling of memory requirements. By trading the precise knowledge of the wavefunction for answers to specific questions, i.e. by the use of Quantum Monte Carlo methods (QMC) to estimate specific correlation functions, we may not only push further in particle number but also to higher-dimensional systems, which has led to great success in spin- and mass-balanced systems. As one moves to mass-imbalanced systems, however, further restrictions appear, namely the infamous sign problem, and computational effort is again prohibitive.

One way to circumvent the exponentially large computational cost at finite mass difference is to “take a detour via the complex plane”. Motivated by the use of an imaginary chemical potential in the investigation of the QCD phase diagram [27], it was recently shown that the same idea also is useful for nonrelativistic fermions in 3D [28] and 1D [29] at finite temperature. A natural move from imaginary polarization is the step to imaginary mass imbalance, which was investigated in Ref. [30] and later applied to the ground state of a unitary Fermi gas on the lattice [31]. Another approach to circumvent the sign problem by using complex numbers is the so-called complex Langevin (CL) method, which is a complex generalization of the idea of stochastic quantization. Considerable progress was made in the last decade in understanding when that method is valid and useful for relativistic theories (see e.g. Refs. [32–35]) as well as for nonrelativistic systems (see e.g. Refs. [36–38]).

Below, we first describe the model underlying our studies, relevant scales, and dimensionless parameters, and elaborate on both the imaginary-mass and CL approaches. After that, we present our results for the ground-state energy and compare the two methods at finite mass imbalance in the case of attractive interactions in Sec. IV. In the same section, our main result, namely the equation of state as a function of both mass imbalance and interaction strength (both attractive and repulsive) is shown. We summarize and present our conclusions in the last section.

II. MODEL, SCALES, AND PARAMETERS

In this work we focus on nonrelativistic 1D fermions with contact interaction among the spin species, which are governed by the Hamiltonian

$$\hat{H} = \hat{T} + \hat{V}, \quad (1)$$

with

$$\begin{aligned} \hat{T} &= \sum_{s=\uparrow,\downarrow} \int dx \, \hat{\psi}_s^\dagger(x) \left(-\frac{\hbar^2}{2m_s} \partial_x^2 \right) \hat{\psi}_s(x), \\ \hat{V} &= g \int dx \, \hat{\psi}_\uparrow^\dagger(x) \hat{\psi}_\uparrow(x) \hat{\psi}_\downarrow^\dagger(x) \hat{\psi}_\downarrow(x). \end{aligned} \quad (2)$$

Here, $\hat{\psi}_s^\dagger(x)$ and $\hat{\psi}_s(x)$ denote operators that create and annihilate fermions of spin s , respectively. Note the spin dependence of the mass in the kinetic part \hat{T} renders the model insoluble, as opposed to the integrable Gaudin-Yang model [39].

The above expressions describe dilute Fermi gases when the effective interaction range r_0 is much smaller than the average interparticle distance $\sim k_F^{-1}$, with $k_F = \frac{\pi}{2}n$ being the Fermi momentum. In such systems, the sole physical parameter describing the interaction between particles is the s -wave scattering length a which is connected to the coupling through $g = 2/a$ (see e.g. Ref. [40]). In our case, additional physical input are the total particle number $N = N_\uparrow + N_\downarrow$ and the box size L , which we use to define the conventional dimensionless coupling $\gamma = g/n$, with $n = N/L$ being the particle density.

From now on, we work in units such that $k_B = \hbar = 1$ and normalize our results for the ground-state energy using the energy of the noninteracting mass- and spin-balanced Fermi gas in the continuum

$$E_{\text{FG}} = \frac{1}{3} N \epsilon_F, \quad (3)$$

where $\epsilon_F = k_F^2/2$. To simplify the discussion of mass imbalanced systems, we define the dimensionless mass-imbalance parameter

$$\bar{m} = \frac{m_\uparrow - m_\downarrow}{m_\uparrow + m_\downarrow}, \quad (4)$$

which is consistent with the literature [30, 31]. Note that the system is invariant under $\bar{m} \rightarrow -\bar{m}$ as long as the system is unpolarized, which is always the case in this work.

III. MANY-BODY METHODS

Here we present the essential ingredients of our ground-state formalism for Fermi gases with short-range interactions described by Eq. (2). We start with the approach previously employed to 1D, 2D, and 3D Fermi gases with equal masses and attractive interaction on a lattice with periodic boundary conditions [13, 41, 42]. The partition sum \mathcal{Z}_β is written as

$$\mathcal{Z}_\beta = \langle \psi_0 | e^{-\beta \hat{H}} | \psi_0 \rangle \equiv \langle \psi_0 | \hat{\mathcal{U}}_\beta | \psi_0 \rangle, \quad (5)$$

which projects the guess state $|\psi_0\rangle$ onto the ground state in the limit $\beta \rightarrow \infty$. Here, β refers to the extent of the

imaginary time direction. The central object to compute is the transfer matrix $\hat{\mathcal{U}}_\beta$, which is challenging for any nontrivial \hat{H} because \hat{T} and \hat{V} do not commute. To deal with the two-body operator \hat{V} , a discretization of the imaginary time axis is performed followed by symmetric Trotter-Suzuki factorization [43]. This is in turn followed by a Hubbard-Stratonovich (HS) transformation to replace the quadratic occurrence of the density operator with a linear one coupled to an auxiliary field $\sigma(x, \tau)$ (see Refs. [44]). Eventually, these steps yield the following path integral:

$$\mathcal{Z}_\beta = \int \mathcal{D}\sigma \det U_\beta^\uparrow[\sigma] \det U_\beta^\downarrow[\sigma]. \quad (6)$$

The determinants in the above expression are taken over the single-particle representation of the respective (HS-transformed) transfer matrices $U_\beta^s[\sigma]$, which reflects the use of a Slater determinant as a trial state $|\psi_0\rangle$ (see Ref. [45]). It is crucial for conventional Monte Carlo approaches that the product of these determinants be non-negative, since only then one may interpret the integration kernel as a probability measure:

$$\mathcal{Z}_\beta \equiv \int \mathcal{D}\sigma P[\sigma] \equiv \int \mathcal{D}\sigma e^{-S[\sigma]}. \quad (7)$$

Here, we defined the action $S[\sigma] = -\ln P[\sigma]$, which is real only when $P[\sigma]$ is positive. To evaluate the path integral, we apply the *hybrid Monte Carlo* (HMC) algorithm [46], which is an essential method for lattice QCD calculations. The objective of HMC is to perform global updates on the auxiliary field σ as opposed to a number of random local updates. This goal is achieved by introducing a conjugate momentum field $\pi(x, \tau)$ and multiplying the path integral by an immaterial constant factor:

$$\mathcal{Z}_\beta \equiv \int \mathcal{D}\pi \int \mathcal{D}\sigma e^{-\mathcal{H}[\sigma, \pi]}, \quad (8)$$

where

$$\mathcal{H}[\sigma, \pi] \equiv S[\sigma] + \int dx \int d\tau \frac{1}{2} [\pi(x, \tau)]^2. \quad (9)$$

To obtain an updated field configuration, the equations of motion, given by

$$\begin{aligned} \frac{\partial \sigma}{\partial t} &= \frac{\delta \mathcal{H}}{\delta \pi} = \pi, \\ \frac{\partial \pi}{\partial t} &= -\frac{\delta \mathcal{H}}{\delta \sigma} = -\frac{\delta S[\sigma]}{\delta \sigma} \end{aligned} \quad (10)$$

are integrated along a trajectory of length ~ 1 in the fictitious HMC time t . By this on-shell propagation of the auxiliary-field, governed by the auxiliary classical Hamiltonian $\mathcal{H}[\sigma, \pi]$ (whose value is preserved throughout the evolution), the acceptance rate for the Metropolis accept-reject step is almost 100%, as the same Hamiltonian \mathcal{H} is used to decide that step. The latter is allowed because,

as noted above, the introduction of the field π into the action is immaterial to the dynamics of the system. Indeed, it factors out of \mathcal{Z}_β completely.

To calculate physical observables we can take derivatives with respect to associated source terms introduced in the action $S[\sigma]$. In this work, we focus on the ground-state energy, which we obtain by taking a log-derivative of the partition sum with respect to imaginary time:

$$E_\beta = -\frac{\partial \ln \mathcal{Z}_\beta}{\partial \beta} = -\frac{1}{\mathcal{Z}_\beta} \frac{\partial \mathcal{Z}_\beta}{\partial \beta}. \quad (11)$$

As mentioned above, for a method based on importance sampling [47], a positive probability measure $P[\sigma]$ in Eq. (7) needs to be guaranteed, or in other words: the action $S[\sigma]$ must be real. This is only the case for systems with an even number of equally populated spin species with uniform masses. In this case, the transfer matrices of all spin species are equal. Additionally, within our approach, it is necessary for the interaction to be attractive such that the operator $\hat{\mathcal{U}}_\beta$ in Eq. (5) is real. For any other fermionic system our QMC-based approach is subject to the infamous sign problem, rendering the simulation time exponentially growing in system size (particle number or spatial extent, depending on the specific algorithm). Below, we elaborate on the two methods used here to circumvent the sign problem for systems of fermions with unequal masses as well as repulsive interactions.

A. Imaginary mass-imbalance

As outlined in the previous section, it is necessary to provide a non-negative integral kernel in Eq. (7) to enable QMC sampling. By choosing the masses of the particles to be complex and such that they satisfy the condition $m_\uparrow = m_\downarrow^*$, one can show that the transfer matrices $U_\beta^\uparrow[\sigma]$ and $U_\beta^\downarrow[\sigma]$ for spin-up and -down fermions are complex conjugate of each other. It is instructive to write the masses as

$$\begin{aligned} m_\uparrow &= m_0 + i\frac{\delta m}{2}, \\ m_\downarrow &= m_0 - i\frac{\delta m}{2}, \end{aligned} \quad (12)$$

which using Eq. (4) yields

$$\bar{m} = i\frac{\delta m}{2m_0}. \quad (13)$$

In the following, we set $m_0 = 1$ which fixes the scale for the masses in our calculations.

With these definitions, the product of the determinants can be written as an absolute square and thus remains positive semidefinite for arbitrary imaginary mass asymmetry:

$$P[\sigma] = \det U_\beta^\uparrow[\sigma] \det U_\beta^\downarrow[\sigma] = |\det U_\beta^\uparrow[\sigma]|^2. \quad (14)$$

The partition sum (6) can now be obtained via standard QMC methods and we are able to extract observables as a function of the imaginary mass imbalance \bar{m} . In order to obtain physical results, however, we need to perform an analytic continuation to real mass imbalance via e.g. a polynomial fit or a fit to a Padé approximant. Strictly speaking, such a continuation to the real plane is only defined if the partition sum \mathcal{Z}_β is an analytic function of \bar{m} , a fact that is not trivially confirmed in practice. To gain analytic insight, however, we discuss below the noninteracting Fermi gas along with our results using the QMC approach discussed above.

It is important to note here that this approach is fully nonperturbative. The results do contain systematic uncertainties, but those are by definition controllable as they arise from the discretization of spacetime. Naturally, the analytic continuation has limitations and actually fails at very high mass imbalances [31], as we will also discuss below. For low to intermediate mass-imbalances, however, the use of imaginary mass-imbalances enable the calculation of few- to many-body properties of Fermi gases in arbitrary dimension. Below, we will use the abbreviation iHMC to refer to the above approach of combining HMC data at imaginary \bar{m} followed by analytic continuation.

B. Complex Langevin dynamics

Instead of adapting the method such that a positive probability measure is guaranteed, one may rethink the update process of the auxiliary field σ altogether. More specifically, we may let σ evolve according to a different equation of motion

$$\frac{\partial \sigma(t)}{\partial t} = -\frac{\delta S[\sigma]}{\delta \sigma} + \eta(t), \quad (15)$$

i.e. the *Langevin equation*. Here, t is a fictitious Langevin time and η comprises a random noise field with expectation value $\langle \eta(t) \rangle = 0$ and autocorrelation $\langle \eta(t)\eta(t') \rangle = 2\delta_{t,t'}$. The above expression is borrowed from the context of statistical physics, where it describes the stochastic movement of a heavy (slow) particle immersed in a rapidly changing background of lighter (fast) particles, i.e. the *Brownian motion*. In a computational context, on the other hand, the use of Eq. (15) is termed (real) *Langevin dynamics* (RL), whose foundation lies in the concept of *stochastic quantization*. The latter interprets the stationary distribution of a stochastic process as the probability measure in the path integral of the corresponding Euclidian field theory [48].

Although the RL algorithm is again restricted to real actions, complex actions can be considered by complexifying the auxiliary field σ . We then obtain a new set of

equations of motion [49]:

$$\begin{aligned} \frac{\partial \sigma_R(t)}{\partial t} &= -\text{Re} \left[\frac{\delta S[\sigma]}{\delta \sigma} \right] + \eta(t), \\ \frac{\partial \sigma_I(t)}{\partial t} &= -\text{Im} \left[\frac{\delta S[\sigma]}{\delta \sigma} \right]. \end{aligned} \quad (16)$$

Unfortunately, there is no rigorous mathematical foundation for the CL approach and despite its elegance there are two caveats with the method. First of all, convergence is not guaranteed due to numerical instabilities and, even if convergence is achieved, it is not certain that the correct result is reproduced. The former difficulty is of numerical nature and has been cured by using adaptive time-step solvers [33]. The issue regarding the correctness of the result is much more delicate and is due to singularities in the imaginary part of the auxiliary field [34, 35, 50]. More precisely, these singularities occur in our case through the use of an HS transformation that depends on $\sin \sigma$:

$$\sin \sigma = \sin \sigma_R \cosh \sigma_I + i \cos \sigma_R \sinh \sigma_I. \quad (17)$$

Thus, the imaginary direction is not bounded and expectation values of observables must be assumed to be contaminated by singularities i.e. cannot be trusted without further analysis even if convergence is achieved.

To prevent the CL algorithm from uncontrolled “excursions” in the complex plane, the insertion of a “regulator” in the equation of motion was proposed recently [38]. The discretized equations of motion then read

$$\begin{aligned} \delta \sigma_R &= -\text{Re} \left[\frac{\delta S[\sigma]}{\delta \sigma} \right] h_t - 2\xi \sigma_R h_t + \eta \sqrt{h_t}, \\ \delta \sigma_I &= -\text{Im} \left[\frac{\delta S[\sigma]}{\delta \sigma} \right] h_t - 2\xi \sigma_I h_t, \end{aligned} \quad (18)$$

where h_t is the (adaptive) step size in CL time t . The parameter ξ determines the strength of the regulating term which can be thought of as a damping force that keeps the auxiliary field from wandering to large values of σ . Of course, this term represents a systematic influence whose effect needs to be studied carefully. Practically, we can calculate observables at different values of ξ and then consider the extrapolation $\xi \rightarrow 0$. We have checked this issue carefully and observe the same convergence pattern as reported in Ref. [38]. In our explicit calculations, we have found that ξ has to be chosen such that the regulator term is rendered sufficiently large compared to the average magnitude of the drift term $\sim \delta S/\delta \sigma$. At the same time, we also have to keep ξ sufficiently small to ensure that the regulator term does not exceed the average magnitude of the drift term and therefore dominates the physics.

Although several runs at different values of ξ are needed to obtain results, this procedure only introduces a linear increase of computational effort as the simulation time of a single run does not depend on the value of ξ explicitly. To illustrate the extrapolation procedure,

we show in Appendix A how the energy of a Fermi gas with $\bar{m} = 0.3$ and $\bar{m} = 0.6$ has been extracted from the numerical data obtained with different values of ξ . In addition, a discussion of the role of the parameter h_t controlling the (adaptive) step size in Eq. (18) can be found in Appendix A as well.

Using Eq. (18), it is possible to estimate path integrals that would be subject to a sign-problem in conventional QMC approaches. Thus, we have a method at hand to study, in a fully nonperturbative way, many-body systems of mass- and spin-imbalanced Fermi gases, at least potentially without constraints on any imbalance parameters. In the following, we apply the method to 1D fermions with arbitrary mass imbalance and underline its correct behavior by comparison with other approaches.

Like iHMC, the CL method involves systematic uncertainties associated with the discretization of spacetime, which are controllable. While no analytic continuation is involved, it should be stressed that the CL method remains a method “under construction” in the sense that its mathematical underpinning is still under development. However, we interpret the remarkable agreement between CL and iHMC for mass-imbalanced systems, and between CL and a renormalization-group approach across a wide range of interaction strengths (including repulsive couplings), as strong evidence that our CL approach works for the systems studied here, see our discussion below.

IV. RESULTS AND DISCUSSION

In this section we present our fully nonperturbative results for the ground-state energy of interacting fermions of unequal masses. Wherever possible, we compare our results to those obtained by other methods. Additionally, we show the equation of state for the ground-state energy as a function of (attractive and repulsive) interaction strength across a wide range of mass imbalances. To our knowledge, this is the first determination of the full equation of state for mass-imbalanced fermions interacting via a contact interaction in one dimension.

In the following, all values will be shown as dimensionless quantities relative to the ground-state energy of the noninteracting system *in the continuum* $E_{FG} = \frac{1}{3}N\epsilon_F$ at the same density and particle number. We set the number of 1D spatial lattice sites to $N_x = 40$, which we found to be sufficient for the methodological purpose of the present work, see also Ref. [14] for a study of the N_x scaling behavior of 1D mass-balanced Fermi gases. The spatial lattice spacing is fixed to unity, which sets the length and momentum scales in our problem. The temporal lattice spacing was chosen to be $\tau = 0.05$ and is sufficient to study the interaction strengths under consideration [13]. Furthermore, we numerically extrapolate to the limit of large imaginary time $\beta\epsilon_F$ by fitting a constant to a few values obtained at sufficiently large propagation times (following Ref. [13]) to save numerical effort. To carry out that extrapolation, we performed calculations

on temporal lattices as large as $N_\tau \sim 1500$, which we found in previous work to be sufficient for the particle numbers and couplings considered here [13]. Each data point shown was computed using an average of 5000 decorrelated samples (both in the iHMC and CL approaches).

A. Imaginary mass imbalance

In order to study the interacting Fermi gas, it is instructive to first investigate its noninteracting counterpart. To calculate the noninteracting energy on the lattice, we simply sum the single-particle energies and as a function of the mass imbalance \bar{m} we obtain

$$E_{\bar{m}} = E_0 \left[\frac{1}{1 - \bar{m}^2} \right] = E_0 \left[\frac{1}{1 + (-i\bar{m})^2} \right], \quad (19)$$

where E_0 is the corresponding noninteracting energy for mass-balanced systems *on the lattice*. This expression is symmetric in \bar{m} , as it should be, since we investigate equally populated spin species. Note also that the energy as obtained from a calculation in the mean-field approximation exhibits the same dependence on \bar{m} as detailed here for the noninteracting system (see, e.g., Ref. [31]).

The top panel of Fig. 1 shows our results for the ground-state energy (black diamonds) for various couplings as function of imaginary \bar{m} along with the noninteracting line (solid black) according to Eq. (19). The noninteracting form suggests the use of a Padé approximant fit to the data, which takes the form

$$f(\bar{m}) = \frac{\sum_{i \geq 1} b_i \bar{m}^{2i}}{1 + \sum_{j \geq 1} c_j \bar{m}^{2j}}, \quad (20)$$

where the even powers reflect the symmetry under $\bar{m} \rightarrow -\bar{m}$, and the b_j ’s and c_j ’s are fit parameters. The colored lines in Fig. 1 represent a least-squares fit of the above form with a polynomial of order 2 (4) in the numerator (denominator). The nearly perfect agreement with the numerical data is crucial when performing an analytic continuation to real \bar{m} as small variations in the fit parameters can greatly influence the final results for real mass imbalances. In principle, higher orders can be included in the polynomials; however, we have found that doing this limits the stability of the fit procedure. Therefore, we only use the before-mentioned order of the Padé approximant in this work.

To obtain results for real \bar{m} , we perform an analytic continuation to the real axis via

$$i\delta m \rightarrow \delta m \quad (21)$$

which implies

$$\bar{m} \rightarrow \frac{\delta m}{2m_0}. \quad (22)$$

The results of the analytic continuation are shown in the bottom panel of Fig. 1 along with the 95% confidence

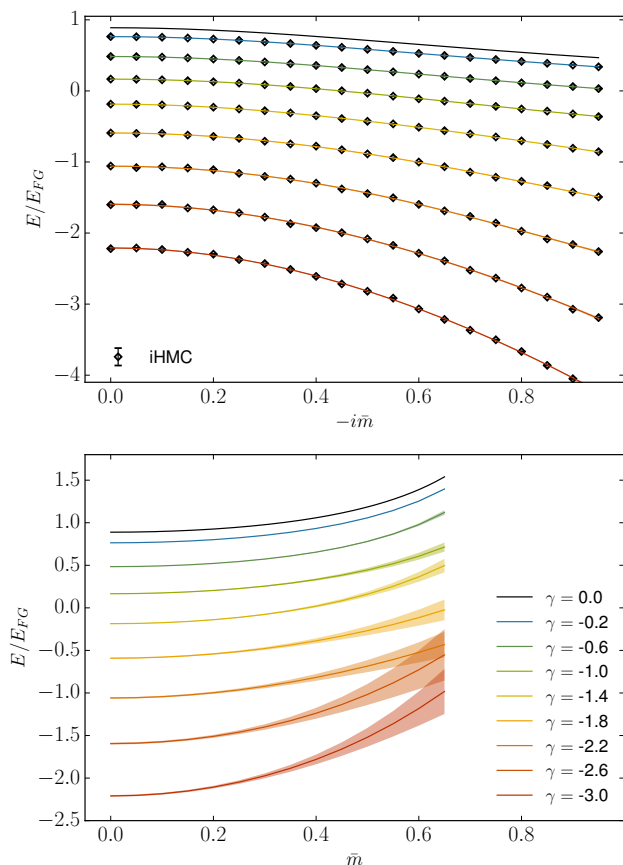


FIG. 1. Ground-state energy of $N = 3 + 3$ fermions as a function of imaginary (top) and real (bottom) mass imbalance for various couplings γ from weak to strong attractive interaction (lines ordered from top to bottom). Top: iHMC results for imaginary \bar{m} (black diamonds, statistical error bars are of the size of the symbols) with Padé approximations according to Eq. (20) (solid colored lines). The black solid line shows the noninteracting result on the lattice. Bottom: analytically continued ground-state energies as a function of real mass imbalance (solid lines). Although the fits as a function of imaginary mass imbalance are precise, small uncertainties result in wide confidence bands (shaded areas) when displayed as a function of real mass imbalance. The plot range in the bottom panel was limited to $\bar{m} = 0.65$ due to large uncertainties beyond that point.

level (shaded). We find very good agreement with the form of the noninteracting result (solid black line) and the results for the energies are very stable with the order of the Padé approximant up to $\bar{m} \sim 0.5 \dots 0.6$. For mass imbalances beyond $\bar{m} \sim 0.6$, however, the associated uncertainties grow rapidly and a quantitative prediction for the ground-state energy (or any other observable) is not guaranteed, particularly at strong couplings. At very high imbalances (not shown in this plot), it is even possible that the qualitative trend as a function of \bar{m} changes due to the effect of the higher-order terms in the functional form of the fit. A possible solution to this issue may be to use a larger amount of data and a finer grid

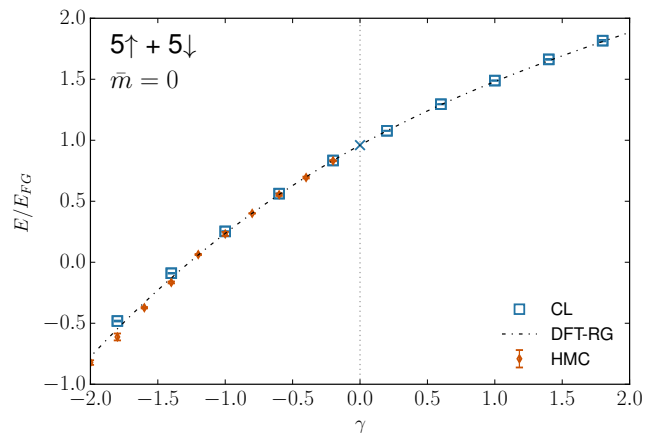


FIG. 2. Ground-state energy of $N = 5 + 5$ fermions of equal mass ($\bar{m} = 0$) as a function of interaction strength computed with iHMC (red error bars), CL (blue squares), and DFT-RG (dash-dotted line).

for the $(-i\bar{m})$ -axis. While this is feasible (albeit tedious) in 1D, the numerical effort in 2D and 3D would be definitely prohibitive.

B. Complex Langevin approach

In this section we present our results obtained with the CL approach, as introduced above, and benchmark our results with those from our iHMC study and (semi) analytic calculations. In what follows, we discuss results for the strength of the regulating term to be $\xi = 0.1$ and the target CL integration step $h_0 = 0.01$. From an analysis of the dependence of our results on these parameters, we found that these values are well suited to study the ground-state energy within a precision on the 1% level. We stress, however, that those values could change when considering different quantities such as correlation functions and density matrices.

1. Mass balanced case: Arbitrary interaction

We begin by considering the mass-balanced scenario, which provides a valuable cross-check as such systems are accessible with a variety of other methods. In particular, we compare our results to those previously obtained with HMC in Ref. [13] for attractive systems which have also been found to agree with exact results from the Bethe ansatz. Additionally, we show results from a renormalization-group approach to density functional theory based on the microscopic interactions defining our model [51]. We will abbreviate this approach as DFT-RG which was put forward in Refs. [52–54]. As shown in Fig. 2, we find outstanding agreement among all methods for $-2 \lesssim \gamma < 0$ (attractive coupling). Moreover, the results from our CL study and those from the DFT-RG

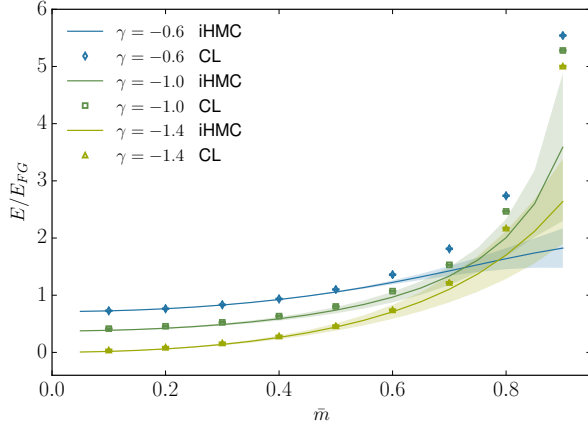


FIG. 3. Ground-state energy of $N = 5+5$ fermions computed using iHMC (solid lines) and CL (symbols). The shaded areas represent the 95%-confidence interval of iHMC data, the uncertainties in the CL data are smaller than the symbol sizes. We find agreement in the ground-state energies at low imbalances up to $\bar{m} \sim 0.5$. Beyond that point the higher-order terms in the Padé approximants reduce the curvature of the iHMC lines. The energies calculated with CL increase monotonically as \bar{m} approaches unity as naively expected for a species with diverging kinetic energy (zero mass).

approach also agree very well for the repulsive case in the regime $0 < \gamma \lesssim 2$, where our QMC approach is bound to fail due to the sign problem. Note that $|\gamma| \lesssim 2$ is roughly the range where the DFT-RG approach is able to formulate reliable predictions based on state-of-the-art truncations presently restricted to mass-balanced systems.

2. Mass imbalanced case: Comparison with iHMC

Motivated by the excellent agreement between CL and other methods in mass-balanced systems, we expand our investigation to mass-imbalanced systems using the CL approach. As mentioned above, there is no need for analytic continuation, which saves in computational effort since we only have to compute single data points (as opposed to a grid of data points which is then fitted). Although it is possible to run calculations for an arbitrary configuration of the fermion masses m_\uparrow and m_\downarrow , we stick to the definition Eq. (12) introduced with the iHMC method to facilitate a straightforward comparison.

Our CL results are shown in Fig. 3 for various attractive coupling strengths on top of results from iHMC calculations for the same parameter values. We find excellent agreement between the methods up to $\bar{m} \sim 0.5-0.6$, which is where the iHMC algorithm incurs large uncertainties (as mentioned in a previous section). Remarkably, the results obtained with the CL algorithm continue to be smooth well beyond that regime and the statistical uncertainties are of roughly constant magnitude across all imbalances considered.

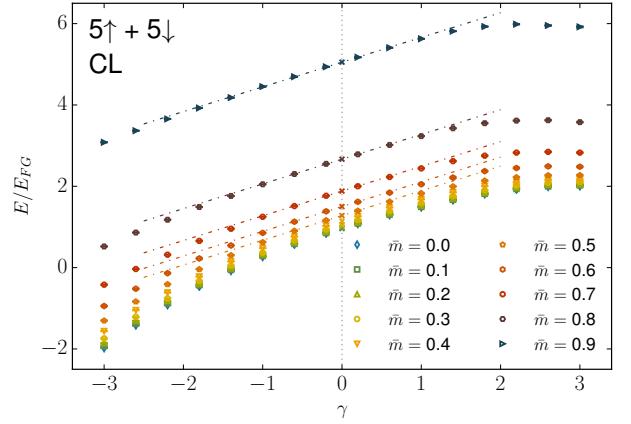


FIG. 4. Ground-state energy of $N = 5 + 5$ fermions as a function of the dimensionless coupling γ for several mass imbalances \bar{m} as obtained from our CL approach. Error bars are of the size of the symbols and below. The dashed-dotted lines show the first-order perturbative result of Eq. (23).

3. Equation of state for arbitrary mass imbalance

Thus far, we have compared our CL results to various methods and found excellent agreement for all cases considered. Most of parameter space, however, is generally difficult to access due to analytic and numerical problems, as pointed out above. The CL method is, however, able to predict values for arbitrary \bar{m} and across a wide range of both attractive *and* repulsive interaction strengths, although the results for strong repulsion ($\gamma \gtrsim 1$) have to be taken care with some care at present as we discuss in Appendix B. To underscore this ability, we present in Fig. 4 our determination of the equation of state for mass-imbalanced fermions. As can be appreciated in the figure, the results are smooth as a function of interaction strength and mass imbalance and intersect the correct noninteracting results on the vertical line at $\gamma = 0$.

It is also evident in Fig. 4 that the equation of state becomes linear in a region around $\gamma = 0$. This linear region can be compared with a first-order perturbative calculation of the ground state energy, as shown in Fig. 4, which is given by

$$\frac{E}{E_{FG}} = \frac{E_{\bar{m}}}{E_{FG}} + \gamma \frac{24}{\pi^2} \frac{N_\uparrow N_\downarrow}{(N_\uparrow + N_\downarrow)^2} + \mathcal{O}(\gamma^2). \quad (23)$$

Here, $E_{\bar{m}}$ is as in Eq. (19). Note that the first-order correction in γ does not depend on the mass imbalance \bar{m} , which is reflected in Fig. 4 in the fact that the slope at $\gamma = 0$ does not change as \bar{m} is increased. Moreover, we observe that our numerical data agrees very well with this perturbative result around $\gamma = 0$, indicating that our CL approach indeed works reliably, at least in the weak-coupling limit. Interestingly, we deduce from this comparison that the size of the linear region depends on \bar{m} and the sign of the coupling γ . In fact, the linear region

is not symmetric around $\gamma = 0$ and even appears to increase with increasing \bar{m} for attractive couplings ($\gamma < 0$).

Our results make the versatility of our CL approach evident. In fact, very promisingly, this enables us to predict values for the ground-state energy at couplings and mass imbalances relevant to experimental setups where analytic expressions are not available and stochastic calculations have only been of limited use so far because of the sign problem. Such experiments include for instance mixtures of the fermionic atoms ^6Li and ^{40}K corresponding to $\bar{m} \approx 0.74$ but also mixtures with smaller values of \bar{m} set up from a variety of suitably chosen different fermion species (such as ^6Li , ^{40}K , ^{161}Dy , ^{163}Dy , and ^{167}Er) in the future (see, e.g., Refs. [8–10]).

Finally, it is worth noting a peculiar feature in the equation of state: depending on the actual value of the mass imbalance, the energy flattens with increasing coupling constant (repulsive case) and its derivative with respect to γ appears to vanish in the limit of infinite repulsion. Moreover, the onset of the flattening behavior is shifted to larger coupling when the mass imbalance is decreased. This can be seen explicitly in the results for $5+5$ fermions in Fig. 4 but we also observe such a behavior for systems with $3+3$ and $4+4$ fermions. This does not come unexpected as our results should only exhibit an explicit dependence on the dimensionless coupling γ and \bar{m} in the infinite-volume limit but no dependence on the actual particle number and box size (i.e. the actual density of the system), provided that the box has been chosen sufficiently large. In any case, this flattening behavior is reminiscent of what is sometimes called fermionization, referring to the fact that an interacting system of distinguishable fermions becomes equivalent to a system of noninteracting identical fermions in the limit of infinite repulsion, see, e.g., Refs. [55–57] for a discussion of this feature for mass-balanced systems. Evidence for this behavior has also been observed in experiments [58–61]. While this behavior may naively seem like a mere curious feature, it may actually have many interesting consequences. For example, the derivative of the energy with respect to the coupling is related to Tan’s contact [62, 63], which in turn governs the short-range and high-frequency tails of all correlation functions. However, a detailed analysis of the energy and the correlation functions in this truly nonperturbative regime is beyond the scope of the present work aiming at methodological developments and cross-verification of stochastic methods. A quantitative study of phenomenologically highly appealing effects, such as the observed flattening behavior of the equation of state, is therefore deferred to future work as it requires a detailed study of finite-size effects and the related approach of the numerical data to the thermodynamic limit. Most prominently, it requires a detailed analysis of systematic effects associated with the CL approach in case of strong repulsive couplings $\gamma \gtrsim 1$, see also Appendix B. Still, detailed quantitative studies of at least the onset of this flattening behavior for mass-imbalanced system appears now in reach based on the present developments.

V. SUMMARY AND OUTLOOK

We have computed ground-state properties of 1D Fermi gases by means of two stochastic numerical methods, namely iHMC and CL. Both methods are able to produce fully nonperturbative results. While the iHMC approach performs well for low to intermediate mass imbalances, large mass imbalances remain elusive due to the instability of the analytic continuation. Remarkably, the CL method possesses no such restriction and is capable of producing quantitative results across all mass imbalances. For small mass imbalances, also accessible to our iHMC approach, the corresponding results agree very well. Although this technique has been known for more than three decades, applications are remarkably scarce in nonrelativistic scenarios; our work aims to fill that gap. Moreover, we have shown excellent agreement with other methods wherever possible, including with perturbative results at small coupling γ .

A word of caution may be in order at this point. It is known that the CL method, being still an approach under construction, may converge to an incorrect answer (see e.g. Ref. [34]). It is also possible for the analytic continuation of iHMC results to the real axis to yield an answer that depends strongly on the choice of fit function. However, the fact that both nonperturbative methods yield essentially the same result in wide swath of parameter space (i.e. as a function of both γ and \bar{m}) is remarkable and supports the idea that the answer is indeed correct.

Finally, we have shown the full equation of state as a function of interaction strength and mass imbalance. To the best of our knowledge, there is no previous determination of the equation of state of 1D mass-imbalanced fermions over such a wide range of mass imbalances and coupling strengths. Thus, although more detailed studies of systematic effects are required to push our calculations towards high precision, our main result of Fig. 4 can already be considered as a first prediction for future ultracold atom experiments with Fermi mixtures. In particular, we have found a feature in the equation of state which appears particularly pronounced at intermediate and large mass imbalances where the equation of state starts to flatten and approaches a \bar{m} -dependent constant already at comparatively small values of the coupling, $\gamma \sim \mathcal{O}(3)$, which appears to point to corresponding significant changes in the short-range (or high-frequency) behavior of correlation functions. A detailed analysis of this strong-coupling regime is deferred to future work.

Our use of periodic boundary conditions aims to reproduce the uniform system, which has now been realized in experimental setups with flat-bottom traps [64] in two-dimensional systems. However, our calculations can be straightforwardly extended to harmonically trapped systems, hard-wall confinement, as well as higher dimensions (see, e.g., Refs. [31, 65, 66]). The discussion of these systems, however, is left to subsequent studies.

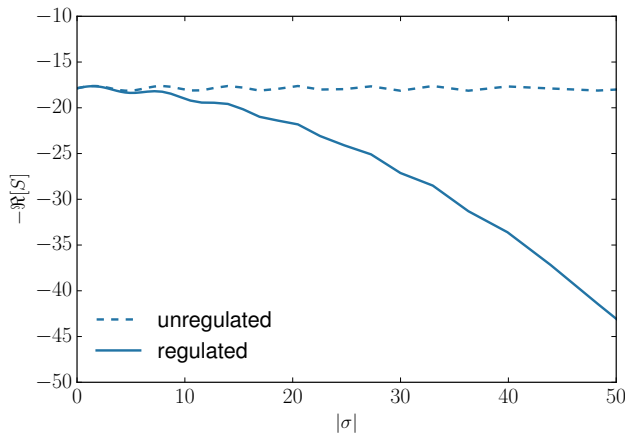


FIG. 5. Real part of the logarithm of the fermion determinant (see Sec. III for our conventions) as a function of the magnitude of the auxiliary field (at a randomly chosen point on the lattice) for an exemplaric choice of parameters (random seed, time of CL evolution, and coupling) for an unregulated (i.e. $\xi = 0$; dashed lines) and an action regulated by choosing $\xi = 0.1$ (solid lines).

ACKNOWLEDGMENTS

This work was supported by HIC for FAIR within the LOEWE program of the State of Hesse and the U.S. National Science Foundation under Grant No. PHY1452635 (Computational Physics Program). Numerical calculations have partially been performed at the LOEWE-CSC Frankfurt. The authors gratefully acknowledge many helpful discussions with A. G. Volosniev.

Appendix A: Effects of the regulator in the complex Langevin approach

In this Appendix we investigate the dependence of our results on two numerical parameters which appear in the CL equations (18): the regulator strength ξ and the step size h_0 entering the solver for the CL equations.

In Ref. [67], it has been shown that the probability measure has to decay sufficiently fast in the limit of large fields σ in order to render the associated CL study reliable. The insertion of a regulator term in our study is related to this issue. Indeed, the regulator term is included to control the excursions in the imaginary direction of the field σ . In Fig. 5, we show $-\mathcal{R}[S]$ as a function of $|\sigma|$ in order to show the result on the action $S[\sigma]$ of scaling up in magnitude the value of σ at a particular location (starting from an otherwise typical field configuration in the CL evolution) which illustrates the necessity of the regulator. Specifically, we show $-\mathcal{R}[S[\sigma]]$, i.e. the real part of the logarithm of the fermion determinant in the absence of the regulator as well as the corresponding answer with the extra term $-\xi \sum_x \sigma^2(x)$ for $\xi = 0.1$. As can be appreciated in the figure, without the regulating

term the action remains at best approximately constant. Even worse, we also find cases where the action grows as the magnitude of σ increases. It is for these reasons that the ξ term is needed.

We now turn our attention to studying the influence of the target step size h_0 and its interplay with the regulator term ξ , and illustrate the extrapolation procedure for two values of the mass-imbalance parameter \bar{m} .

As mentioned in the main part of this work, within the CL approach, it is useful to employ an adaptive step size h_t for the integration of the equations of motion [33]. In our approach, the step size is determined by rescaling the target step size h_0 with the maximum value of the sigma-drift D_{\max} on the spacetime lattice Λ :

$$D_{\max} = \max_{i \in \Lambda} \left| \frac{\delta S[\sigma]}{\delta \sigma} \right|_{\sigma=\sigma_i} - 2\xi\sigma_i \Big|^2. \quad (\text{A1})$$

Naturally, this renders the results dependent on the target step size and appropriate extrapolations to vanishing h_0 are required. In the top panels of Fig. 6, the dependence on h_0 is shown for systems with $N = 5 + 5$ particles with $\bar{m} = 0.3$ and $\bar{m} = 0.6$ on a spatial lattice with $N_x = 40$ sites. Furthermore, data sets for multiple values of the regulator strength ξ are shown. In order to enable a comparison with iHMC results, we consider an attractive coupling. To be specific, we have set the coupling to $\gamma = -1.0$ here, but we add that the general behavior of the CL results for systems with a repulsive interaction is the same. For our extrapolations to vanishing target step size in this work, we have always performed a linear fit of the data which appears to be justified given our data sets, see top panels of Fig. 6 for an illustration. Note that the slope decreases with an increasing regulator strength.

Once the extrapolation to $h_0 = 0$ has been performed for a given system, the dependence of the h_0 -extrapolated values on the regulator strength ξ has to be considered. For the latter, we observe an approximately linear behavior. Therefore, we use again a linear fit to extrapolate $\xi \rightarrow 0$. This is shown in the lower panels of Fig. 6. Remarkably, the extrapolated values agree very nicely with those obtained by our iHMC approach via analytic continuation.

We conclude by noting that the results from these two extrapolations are essentially independent of the order in which they are performed, i.e. if we first extrapolate to $\xi = 0$ and then perform the extrapolation to $h_0 = 0$, we obtain the same results for the energy within the presented error bars.

Appendix B: Distribution of the path-integral measure in the complex Langevin approach

In order to ensure correct convergence of observables calculated with our CL approach, we investigate the distribution of ground-state energies as well as the path integral measure in this appendix. To this end, we consider

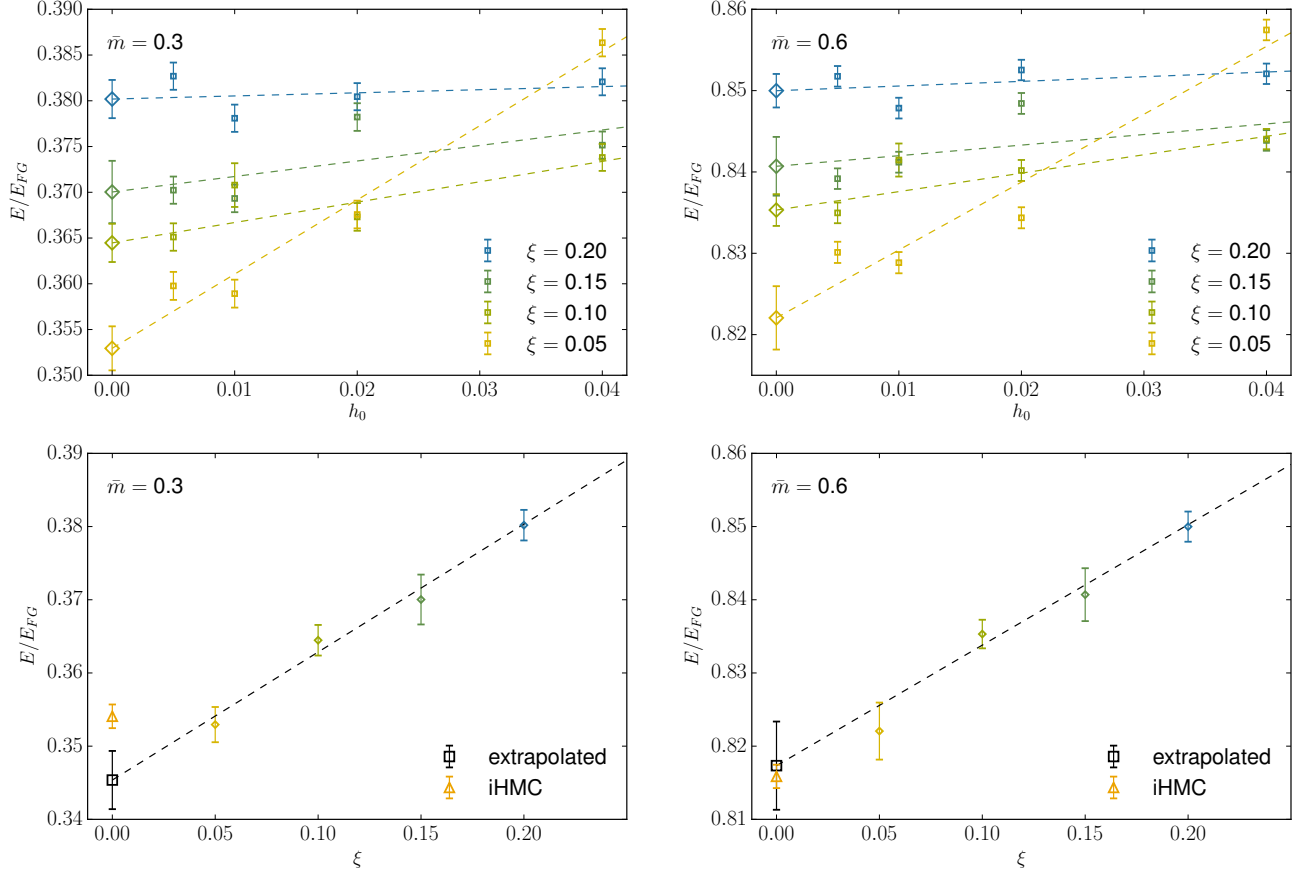


FIG. 6. Top panels: Ground-state energy of a system with $N = 5 + 5$ fermions with mass imbalance $\bar{m} = 0.3$ (top left panel) and $\bar{m} = 0.6$ (top right panel) as a function of the target CL step h_0 for different strengths ξ of the regulating term appearing in the CL equations. The interaction strength is set to $\gamma = -1.0$ in both cases. Dashed lines represent linear fits which have been used to extrapolate to the limit $h_0 \rightarrow 0$. The latter are marked by diamonds. Bottom panels: Ground-state energy of a system with $N = 5 + 5$ fermions with mass imbalance $\bar{m} = 0.3$ (bottom left panel) and $\bar{m} = 0.6$ (bottom right panel) as obtained from an extrapolation to $h_0 = 0$ is shown as a function of the regulator strength ξ . The interaction strength is set to $\gamma = -1.0$ in both cases. Dashed lines represent linear fits of the data. For comparison, we also show the results obtained from our iHMC approach via analytic continuation. Note that, whereas the error bars on the CL data points originate from statistical errors, the error bars on all extrapolated CL values as well as the iHMC values refer to errors from associated fits.

a system composed of $N = 5 + 5$ particles with a mass imbalance of $\bar{m} = 0.6$. The general conclusions, however, are valid also for all other systems studied in this work.

During the evaluation of the results obtained from stochastic methods, such as iHMC and CL, it is instrumental to monitor histograms of the calculated observables in order to gain an insight into the behavior of the simulations. Furthermore, it is common practice to define the error bar as the standard deviation over all samples with an assumed Gaussian distribution. A deviation from such a distribution may hint to systematic errors. In the left panel of Fig. 7, we show the distribution of the ground-state energies for a strongly attractive (top) and strongly repulsive (bottom) case. While the histograms associated with attractive systems follow a Gaussian very closely, the repulsive systems exhibit so-called “fat tails”, i.e. an excessive amount of “outliers” with respect to the assumed normal distribution. In fact, more generally

speaking, we find that the distributions in the latter case do not exhibit a fixed variance. The origin of this problem is depicted in the right panel of Fig. 7, where we show the distribution (as obtained from the CL time evolution) of the real part of the action S : Depending on the absolute value of the coupling, the distribution peaks at small positive to large negative values for attractive systems (from weak to strong attraction). For increasing repulsion, on the other hand, the peak wanders to large positive values and the imaginary part of the action is found to be a flat distribution whereas the imaginary part is strongly localized about zero in the attractive case. Note that an increase of the value of the action corresponds to a decrease of the probability measure e^{-S} . Eventually, we even find that the associated probabilities will decrease below the machine precision ($\sim 10^{-16}$). This unavoidably implies that information is lost and immediately leads to a poor *signal-to-noise ratio*. As a consequence, error bars cal-

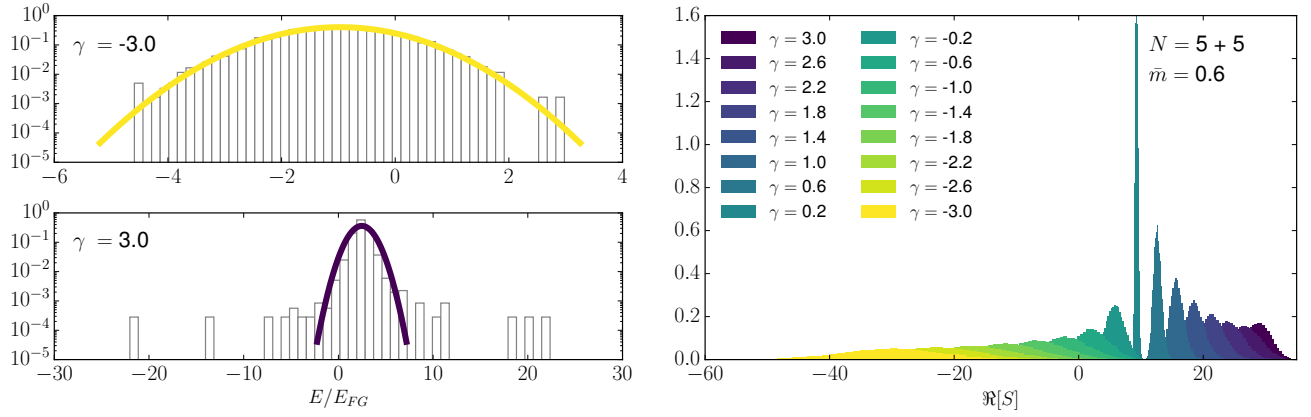


FIG. 7. Left panels: (logarithmic y -scale) of the measured ground-state energies for an attractively (top) and a repulsively (bottom) interacting system. While the former follows a Gaussian distribution, the latter exhibits so-called “fat tails” as a consequence of a *signal-to-noise* problem. Right panel: distributions of the real part of the path integral measure, i.e. the real part of the negative logarithm of the fermion determinant for various systems from strongly attractive to strongly repulsive (from left to right).

culated with the assumption of a Gaussian distribution become unreliable.

The occurrence of signal-to-noise problem is not limited to the CL approach and has been studied for other methods based on a Hubbard-Stratonovich transformation [68] (see also Refs. [69, 70], where a very similar signal-to-noise problem was solved for the calculation of entanglement entropies). Although not implemented in our approach, methods have been proposed to mitigate this issue. Within the CL approach, however, zeroes of the determinant entail $S \rightarrow \infty$ and therefore exhibit an additional problem, namely singularities in the drift term. These singularities, when encountered, possibly spoil the computed expectation values [67]. This may be rated as conceptual problem, in contrast to a vanishing signal due to excessive noise. The latter is at least in principle solvable by (drastically) increasing the sample number. However, note that it may very well be that both problems are related in our case. In fact, a zero

of the determinant yields a vanishing probability which is reminiscent of the situation of strong repulsion as reported above. At present, we cannot resolve whether the CL dynamics at strong repulsive couplings is governed by zeroes of the determinant or whether we only deal with a conventional *signal-to-noise* problem which could at least in principle be solved.

In conclusion, we have found that our simulations yield “fat-tailed distributions” of observables in the repulsive regime (at least for strong repulsion), which are associated with potentially spoiled expectation values. For small to intermediate repulsion ($0 < \gamma \lesssim 1$) the problem appears to be absent or at least strongly suppressed and our results agree very well with DFT-RG, perturbation theory, and exact solutions from the Bethe ansatz [71] where applicable (i.e. for $\bar{m} = 0$). Finally, we have found that our CL approach behaves very well for attractive systems for the studied range of mass imbalances which is not accessible for conventional HMC approaches and exact calculations with the Bethe ansatz.

-
- [1] A. Celi, A. Sanpera, V. Ahufinger, and M. Lewenstein, *Physica Scripta* **92**, 013003 (2017).
 - [2] M. M. Lewenstein, A. Sanpera, and V. Ahufinger, *Ultracold Atoms in Optical Lattices: Simulating Quantum Many-body Systems* (Oxford University Press, New York, 2012).
 - [3] M. A. Cazalilla and A. M. Rey, *Rep. Progr. Phys.* **77**, 124401 (2014).
 - [4] G. Pagano, M. Mancini, G. Cappellini, P. Lombardi, F. Schafer, H. Hu, X.-J. Liu, J. Catani, C. Sias, M. Inguscio, and L. Fallani, *Nat. Phys.* **10**, 198 (2014).
 - [5] A. Trenkwalder, C. Kohstall, M. Zaccanti, D. Naik, A. I. Sidorov, F. Schreck, and R. Grimm, *Phys. Rev. Lett.* **106**, 115304 (2011).
 - [6] F. M. Spiegelhalter, A. Trenkwalder, D. Naik, G. Hendl, F. Schreck, and R. Grimm, *Phys. Rev. Lett.* **103**, 223203 (2009).
 - [7] T. G. Tiecke, M. R. Goosen, A. Ludewig, S. D. Gensemer, S. Kraft, S. J. J. M. F. Kokkelmans, and J. T. M. Walraven, *Phys. Rev. Lett.* **104**, 053202 (2010).
 - [8] R. Grimm, (private communication).
 - [9] M. Lu, N. Q. Burdick, and B. L. Lev, *Phys. Rev. Lett.* **108**, 215301 (2012).
 - [10] A. Frisch, K. Aikawa, M. Mark, F. Ferlaino, E. Berseneva, and S. Kotochigova, *Phys. Rev. A* **88**, 032508 (2013).
 - [11] G. Zürn, A. N. Wenz, S. Murmann, A. Bergschneider, T. Lompe, and S. Jochim, *Phys. Rev. Lett.* **111**, 175302 (2013).

- (2013).
- [12] X.-W. Guan, M. T. Batchelor, and C. Lee, *Rev. Mod. Phys.* **85**, 1633 (2013).
 - [13] L. Rammelmüller, W. J. Porter, A. C. Loheac, and J. E. Drut, *Phys. Rev. A* **92**, 013631 (2015).
 - [14] L. Rammelmüller, W. J. Porter, J. Braun, and J. E. Drut, *Phys. Rev. A* **96**, 033635 (2017).
 - [15] A. G. Volosniev, D. V. Fedorov, A. S. Jensen, M. Valiente, and N. T. Zinner, *Nat. Comm.* **5**, 5300 (2014).
 - [16] A. S. Andersen, M. E. S. and Dehkharghani, A. G. Volosniev, E. J. Lindgren, and N. T. Zinner, *Scientific Reports* **6**, 28362 (2016).
 - [17] N. L. Harshman, M. Olshanii, A. S. Dehkharghani, A. G. Volosniev, S. G. Jackson, and N. T. Zinner, *Phys. Rev. X* **7**, 041001 (2017).
 - [18] M. Olshanii and S. G. Jackson, *J. Phys.* **17**, 105005 (2015).
 - [19] A. S. Dehkharghani, A. G. Volosniev, and N. T. Zinner, *J. Phys. B* **49**, 085301 (2016).
 - [20] A. G. Volosniev, *Few-Body Systems* **58**, 54 (2017).
 - [21] Y.-H. Liu and L. Wang, *Phys. Rev. B* **92**, 235129 (2015).
 - [22] M.-T. Philipp, M. Wallerberger, P. Gunacker, and K. Held, *Eur. Phys. J. B* **90**, 114 (2017).
 - [23] P. Farkasovsky, *Europhys. Lett.* **84**, 37010 (2008).
 - [24] G. G. Batrouni, M. J. Wolak, F. Hébert, and V. G. Rousseau, *Europhys. Lett.* **86**, 47006 (2009).
 - [25] D. Pęcak, M. Gajda, and T. Sowiński, *J. Phys.* **18**, 013030 (2016).
 - [26] D. Pęcak, M. Gajda, and T. Sowiński, *arXiv:1703.08116*.
 - [27] P. de Forcrand and O. Philipsen, *Nucl. Phys. B* **642**, 290 (2002).
 - [28] J. Braun, J.-W. Chen, J. Deng, J. E. Drut, B. Friman, C.-T. Ma, and Y.-D. Tsai, *Phys. Rev. Lett.* **110**, 130404 (2013).
 - [29] A. C. Loheac, J. Braun, J. E. Drut, and D. Roscher, *Phys. Rev. A* **92**, 063609 (2015).
 - [30] D. Roscher, J. Braun, J.-W. Chen, and J. E. Drut, *J. Phys. G* **41**, 055110 (2014).
 - [31] J. Braun, J. E. Drut, and D. Roscher, *Phys. Rev. Lett.* **114**, 050404 (2015).
 - [32] G. Aarts, *Phys. Rev. Lett.* **102**, 131601 (2009).
 - [33] G. Aarts, F. A. James, E. Seiler, and I.-O. Stamatescu, *Phys. Lett. B* **687**, 154 (2010).
 - [34] G. Aarts, E. Seiler, and I.-O. Stamatescu, *Phys. Rev. D* **81**, 054508 (2010).
 - [35] G. Aarts, F. A. James, E. Seiler, and I.-O. Stamatescu, *Eur. Phys. J. C* **71**, 1756 (2011).
 - [36] C. Adami and S. E. Koonin, *Phys. Rev. C* **63**, 034319 (2001).
 - [37] A. Yamamoto and T. Hayata, *PoS LATTICE2015*, 041 (2016), *arXiv:1508.00415*.
 - [38] A. C. Loheac and J. E. Drut, *Phys. Rev. D* **95**, 094502 (2017).
 - [39] M. Gaudin, *Phys. Lett. A* **24**, 55 (1967); C. N. Yang, *Phys. Rev. Lett.* **19**, 1312 (1967).
 - [40] V. E. Barlette, M. M. Leite, and S. K. Adhikari, *Eur. J. Phys.* **21**, 435 (2000).
 - [41] L. Rammelmüller, W. J. Porter, and J. E. Drut, *Phys. Rev. A* **93**, 033639 (2016).
 - [42] J. E. Drut, T. A. Lähde, and T. Ten, *Phys. Rev. Lett.* **106**, 205302 (2011).
 - [43] H. F. Trotter, *Proc. Amer. Math. Soc.* **10**, 545 (1959); M. Suzuki, *Comm. Math. Phys.* **51**, 183 (1976).
 - [44] R. L. Stratonovich, *Soviet Physics Doklady* **2**, 416 (1957); J. Hubbard, *Phys. Rev. Lett.* **3**, 77 (1959).
 - [45] F. F. Assaad and H. G. Evertz, in *Computational Many-Particle Physics*, edited by H. Fehske, R. Schneider, and A. Weiße (Springer Berlin Heidelberg, Berlin, Heidelberg, 2008) p. 277.
 - [46] S. Duane, A. D. Kennedy, B. Pendleton, and D. Roweth, *Phys. Lett. B* **195**, 216 (1987); S. Gottlieb, W. Liu, D. Toussaint, R. L. Renken, and R. L. Sugar, *Phys. Rev. D* **35**, 2531 (1987).
 - [47] N. Metropolis, A. W. Rosenbluth, M. N. Rosenbluth, A. H. Teller, and E. Teller, *J. Chem. Phys.* **21**, 1087 (1953).
 - [48] G. Parisi and Y.-S. Wu, *Sci. Sin.* **24**, 483 (1981).
 - [49] G. Parisi, *Phys. Lett. B* **131**, 393 (1983).
 - [50] L. L. Salcedo, *Phys. Rev. D* **94**, 114505 (2016).
 - [51] S. Kemler, Ph.D. thesis, TU Darmstadt (2017).
 - [52] J. Polonyi and K. Sailer, *Phys. Rev. B* **66**, 155113 (2002).
 - [53] A. Schwenk and J. Polonyi, in *32nd International Workshop on Gross Properties of Nuclei and Nuclear Excitation: Probing Nuclei and Nucleons with Electrons and Photons (Hirschegg 2004) Hirschegg, Austria, January 11-17, 2004* (2004) pp. 273–282, *arXiv:nucl-th/0403011* [nucl-th].
 - [54] S. Kemler and J. Braun, *J. Phys. G* **40**, 085105 (2013); S. Kemler, M. Pospiech, and J. Braun, *ibid.* **44**, 015101 (2017).
 - [55] M. D. Girardeau, *J. Math. Phys.* **1**, 516 (1960).
 - [56] D. S. Petrov, G. V. Shlyapnikov, and J. T. M. Walraven, *Phys. Rev. Lett.* **85**, 3745 (2000).
 - [57] M. D. Girardeau, *Phys. Rev. A* **82**, 011607 (2010).
 - [58] T. Kinoshita, T. Wenger, and D. S. Weiss, *Science* **305**, 1125 (2004).
 - [59] T. Kinoshita, T. Wenger, and D. S. Weiss, *Phys. Rev. Lett.* **95**, 190406 (2005).
 - [60] E. Haller, M. Gustavsson, M. J. Mark, J. G. Danzl, R. Hart, G. Pupillo, and H.-C. Nägerl, *Science* **325**, 1224 (2009).
 - [61] G. Zürn, F. Serwane, T. Lompe, A. N. Wenz, M. G. Ries, J. E. Bohn, and S. Jochim, *Phys. Rev. Lett.* **108**, 075303 (2012).
 - [62] S. Tan, *Ann. Phys.* **323**, 2952 (2008); *Ann. Phys.* **323**, 2971 (2008); *Ann. Phys.* **323**, 2987 (2008).
 - [63] M. Barth and W. Zwerger, *Ann. Phys.* **326**, 2544 (2011).
 - [64] K. Hueck, N. Luick, L. Sobirey, J. Siegl, T. Lompe, and H. Moritz, *arXiv:1704.06315*.
 - [65] C. E. Berger, E. R. Anderson, and J. E. Drut, *Phys. Rev. A* **91**, 053618 (2015).
 - [66] C. E. Berger, J. E. Drut, and W. J. Porter, *Comput. Phys. Commun.* **208**, 103 (2016).
 - [67] G. Aarts, E. Seiler, D. Sexty, and I.-O. Stamatescu, *J. High Energy Phys.* **05**, 044 (2017).
 - [68] H. Shi and S. Zhang, *Phys. Rev. E* **93**, 033303 (2016).
 - [69] J. E. Drut and W. J. Porter, *Phys. Rev. B* **92**, 125126 (2015).
 - [70] J. E. Drut and W. J. Porter, *Phys. Rev. E* **93**, 043301 (2016).
 - [71] N. Oelkers, M. T. Batchelor, M. Bortz, and X.-W. Guan, *J. Phys. A: Math. Gen.* **39**, 1073 (2006).